NANO MICRO small

# Supporting Information

for *Small,* DOI: 10.1002/smll.201501257

# Microengineered $CH_3NH_3PbI_3$ Nanowire/Graphene Phototransistor for Low-Intensity Light Detection at Room Temperature

*Massimo Spina, Mario Lehmann, Bálint Náfrádi, Laurent Bernard, Eric Bonvin, Richard Gaál, Arnaud Magrez, László Forró, and Endre Horváth**

# Supporting Information

**Micro-engineered $CH_3NH_3PbI_3$ nanowire/graphene phototransistor for low intensity light detection at room temperature**

*M. Spina, M. Lehmann, Dr. B. Náfrádi , Dr. L. Bernard, E. Bonvin, Dr. R. Gaál, Dr. A. Magrez,*
*Prof. L. Forró, Dr. E. Horváth**

*Graphene growth.* The graphene used in this work was grown on copper foils via a Chemical Vapor Deposition (CVD) method. First, a 25μm-thick copper foil with lateral dimensions of 2.2 x 5.5 $cm^2$ (Alfa Caesar, 99.8%) was inserted into a 2.5cm-large quartz tube, then placed inside a horizontal tube furnace. After the quartz tube was evacuated to a pressure of 4 mTorr, high purity hydrogen (Carbagas $H_2$, purity 60) was introduced to reach a pressure of 3 Torr. Then, the system was heated to 1000 °C at a rate of 50°C$min^{-1}$ (pressure ~ 900 mTorr). The copper foils were annealed at the growth temperature (1000 °C) in hydrogen for 30 min. A pulsed flow of methane was then introduced to grow the graphene for 3 min. After the growth, the system was cooled down to 300 °C at a rate of 6 °C$min^{-1}$ in a hydrogen atmosphere. Samples were removed from the chamber at temperatures below 300 °C.

*Graphene characterization.* To investigate the quality of the CVD-grown graphene, Raman spectroscopy was performed with a confocal Raman spectrometer (LabRam HR, Horiba Scientific) using a 532nm-laser and a 100x objective lens (spot size of 0.3 μm). From the spectra shown in **figure S1**, we can observe that the G and 2D band points are at 1578 and 2670 $cm^{-1}$ respectively and have a full width at half maximum of 15 and 33 $cm^{-1}$. After the sensitization of the graphene, quantitative analysis of the G and 2D peaks proved difficult because of the intense background signal coming from the photoluminescence of the $MAPbI_3$ nanowires.

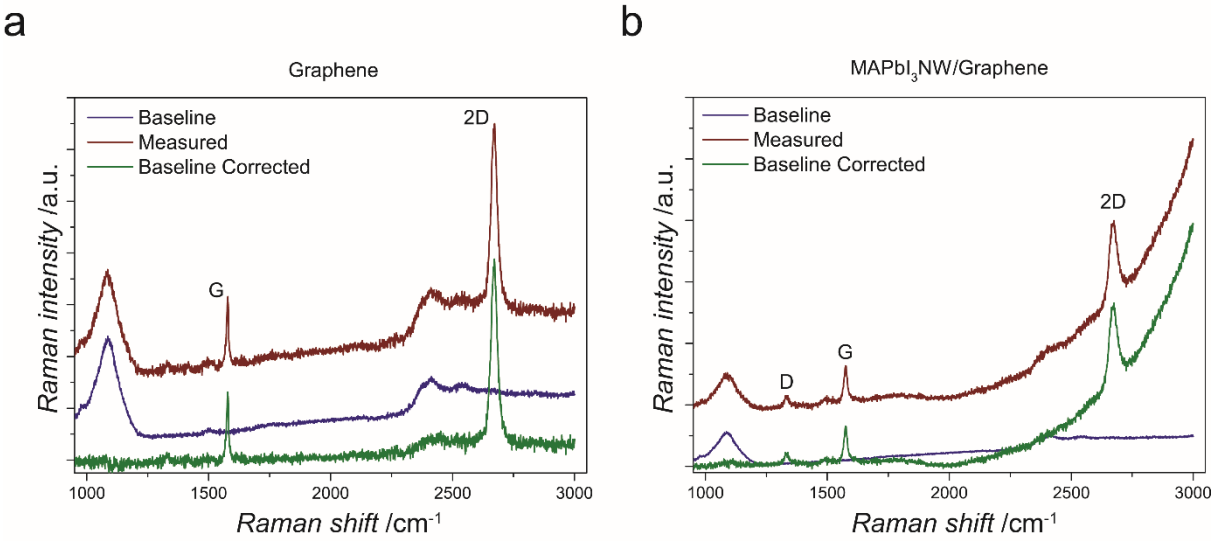


**Figure S1:** Raman spectra of the graphene film (a) and $MAPbI_3$NW/graphene junction (b) used in the study.

*Device Fabrication.* The graphene was transferred onto a highly p-doped Si substrate with a 300nm thick $SiO_2$ layer thermally grown on top by "etching and polymer-supported transfer" method.[1] First, one side of the Cu/graphene film was spin-coated (1000 rpm, 1 min) with a layer of poly(methyl methacrylate) (PMMA, MW 495K). Then, the copper foil was cured 5 min at 180 °C and the non-coated graphene layer was removed using sand paper. The sample was then dipped in an iron chloride solution (20 $mgml^{-1}$) for 7-8 hours in order to etch the copper foil. Later, the graphene/PMMA film was rinsed in a bath of deionized water and in a diluted hydrochloric acid solution to remove the remaining ions. Finally, the graphene/PMMA film was picked up by the substrate, and dried in ambient atmosphere. After the graphene transfer, the PMMA layer used in the process was patterned by e-beam lithography, and employed as an etch mask for patterning the graphene using directional plasma oxygen (100W, 10s, 20sccm $O_2$). The resist was then removed by immersion of the sample in acetone and rinsed in isopropyl alcohol (**figure S2a**). 100nm-thick gold contacts were then patterned by e-beam lithography and thermally evaporated on top of the graphene film (figure S2b). The network of $MAPbI_3$ nanowires was subsequently deposited by the slip- coating technique

reported by Horváth et al.[2] (figure S2c). The devices were then encapsulated in a PMMA layer in order to avoid degradation of the nanowires due to exposure to the ambient atmosphere (figure S2d). The same PMMA layer was patterned by e-beam and used as an etch mask to remove the nanowires located outside the device area using directional Ar ion etch process (figure S2e). A representative diagram of the final device is show in figure S2f.

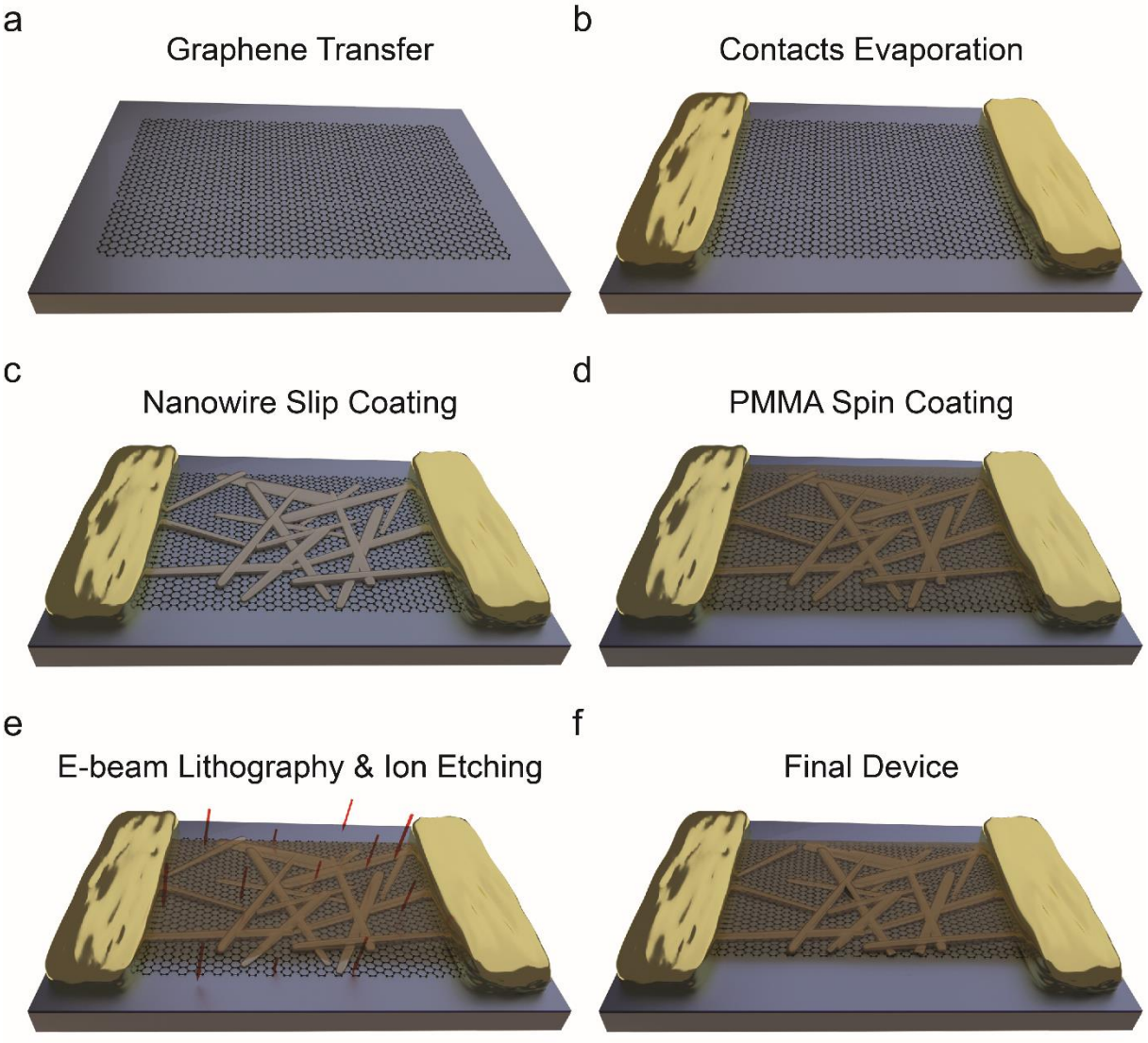


**Figure S2**. (a) The graphene film is transferred on a highly p-doped Si substrate with 300nm $SiO_2$ thermally grown on top. (b) Au contacts are patterned by e-beam lithography and thermally evaporated on the substrate. (c) $MAPbI_3$ nanowires are slip-coated on the patterned graphene film. (d) A film of PMMA is spin coated on the device and used as an etch mask. (e) The nanowires outside the device are etched away by Ar ions. (f) Final device.

*Study of the photoresponse properties of pristine graphene transistor*.

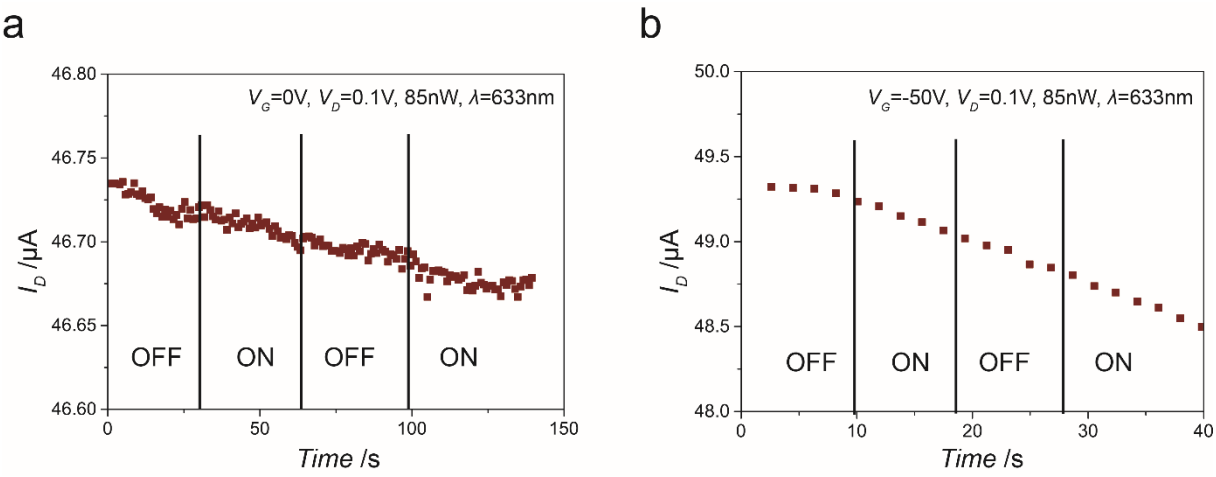


**Figure S3**. Source-to-drain current of a pristine graphene FET for $V_G$=0V (a) and $V_G$=-50V (b). The device was tested by sequencing dark (without illumination, referred as OFF) and illuminated conditions (referred as ON) as a function of time (halogen lamp, 633nm, 42.5nWmm$^{-2}$). Unlike the MAPbI$_3$NW sensitized hybrid devices (Fig. 3b), the pristine graphene does not show any measurable photoresponse at 633 nm illumination.

*Study of the graphene-perovskite interface.* In photovoltaic devices as for every optoelectronic devices, proper contact between electrode and p/n type material is essential in order to have efficient charge collection. To investigate the type of contact between the graphene and the perovskite nanowires we fabricated a photodetector where a network of interconnected $CH_3NH_3PbI_3$ nanowires is contacted by two foils of monolayer graphene acting as the source and drain electrodes (**figure S3a**).

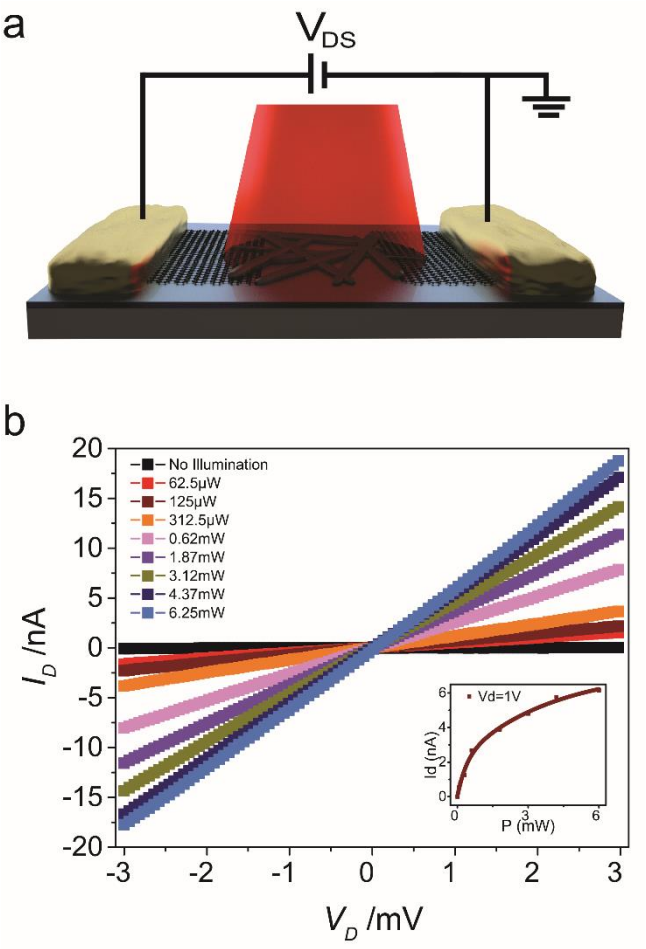


**Figure S4**. (a) Schematic representation of the graphene-nanowires-graphene device. (b) Output characteristics for different power intensities. Graphene contacts show non-rectifying ohmic behavior. The drain current tends to saturate for high laser power intensities but saturation has not been achieved in this study.

The current in the device was measured as a function of the applied source-to-drain voltage in the dark and under illumination of a red laser (λ=633 nm) with a power density of 2.5 $Wcm^{-2}$ (figure S3b). The output characteristics follow a linear behavior, indicating that the contacts between the nanowires and the graphene films are ohmic. In the dark state, the device behaves like a good insulator with currents on the order of tens of pA and resistances in the GOhm range. Under the illumination of the laser, the absorption of the light generates electron-hole pairs that are extracted by the source-to-drain electric field and cause an increase in the

conductance of the material of up to a factor of 500. We probed the photoresponse of the device under different incident laser powers in the 60 µW to 6 mW range and observed a parabolic increase of the current with the incident power intensity (inset to figure S3b).

*Transfer characteristics of graphene-perovskite hybrid transistors in dark and under illumination.*

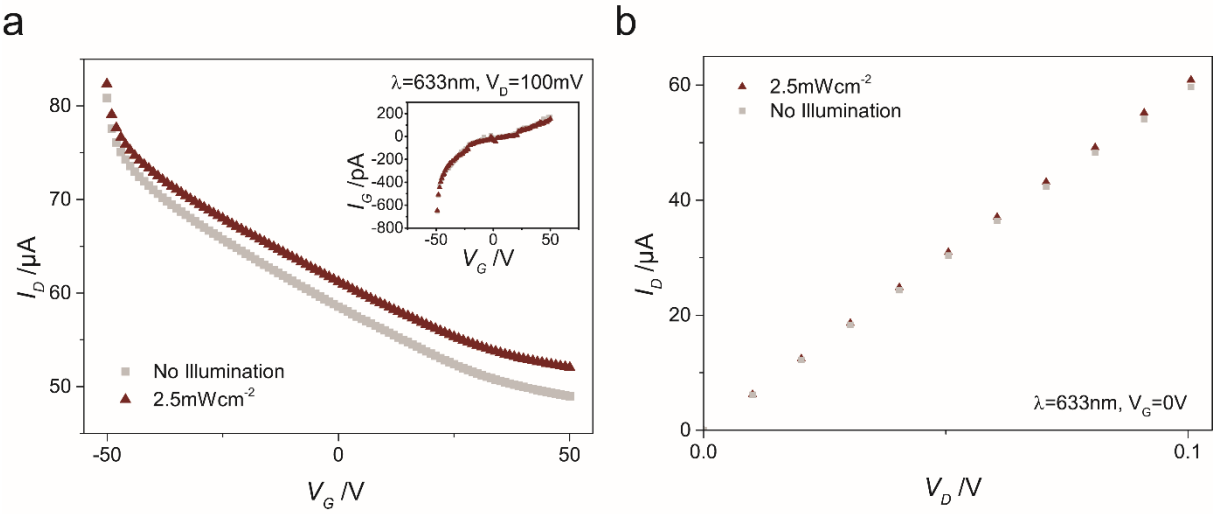


**Figure S5.** Transfer characteristic (a) and output characteristics (b) of our best graphene-perovskite device in dark and under the maximum irradiation power used in our experiments.

In figure S5 we show the dark and light induced characteristics of our best graphene-perovskite hybrid transistor. The properties of the same device are shown in figure 2 in the main text. The current leakage for this device is very low, it stays under 0.7 nA (the gate dependent drain current varies between 50-80 µA). Unlike the drain current (figure S5a main plot) the absolute value of the leakage current does not change under illumination (the red and grey curves overlap in figure S5a inset). The low and relatively stable leakage current excludes the possible artifact, i.e. that the linear enhancement of $I_D$ versus $V_D$ under illumination is not due to a current leaking phenomenon.

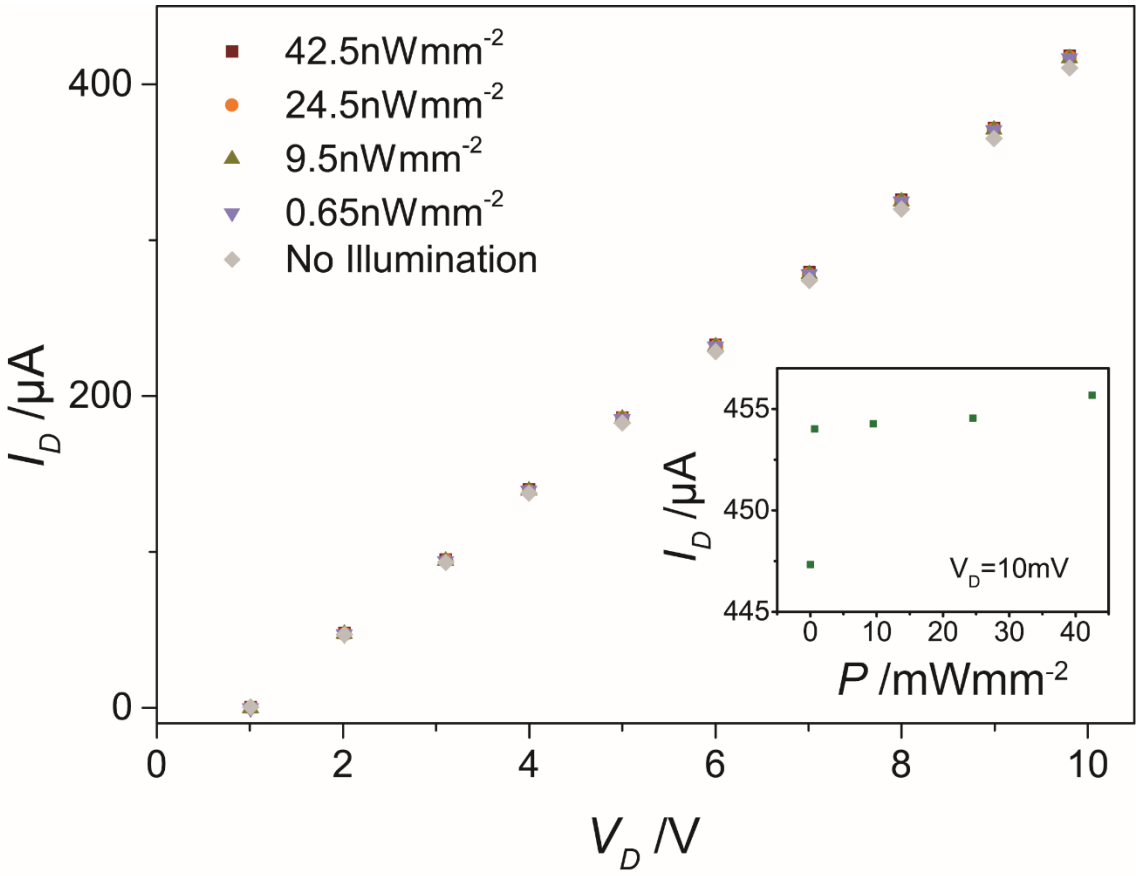


**Figure S6** Dark and light induced characteristics of our best graphene-perovskite hybrid transistor. Here the absolute values of the currents are shown. The properties of the same device is shown in figure 2 in the main text. Note, that in figure 2d the $I_{ph}$ is reported. This is the difference ($I_D$-*light*)-($I_D$-*dark*).

*Calculation of detectivity.* The detectivity measures not only the detectors light conversion efficiency, but also the various noise currents (shot, *1/f*, etc.) introduced by the detection circuit, thus it is not a general materials property. Supposing that the noise current is dominated by the shot noise of the dark current, the detectivity can be expressed as:[3]

$$D^* = \frac{R\sqrt{A}}{\sqrt{2qI_{dark}}}$$

Where $q$ is the elementary charge and $I_{dark}$ is the current passing in the photodiode in dark conditions.

Our best device has an active area of 5000 μm$^2$.

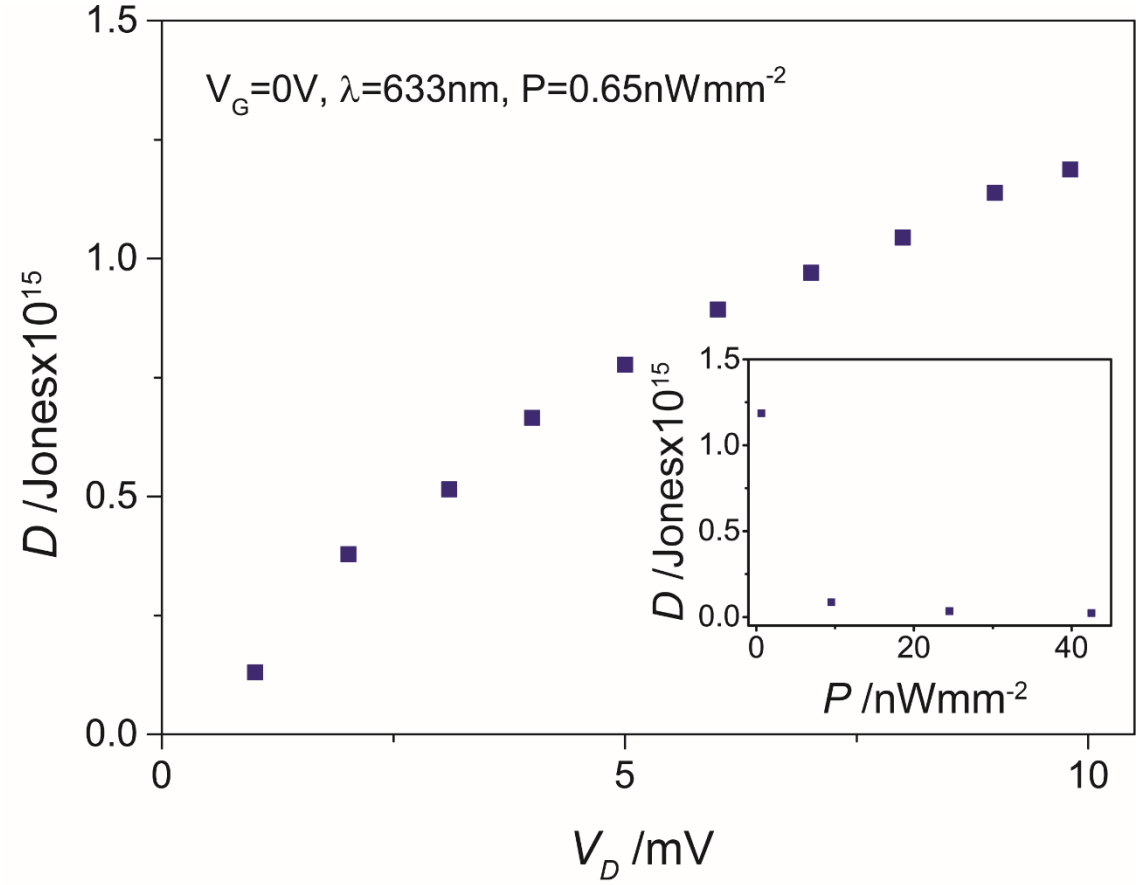


**Figure S7**. Detectivity of the "champion device".

The maximum value of ~1x10$^{15}$ Jones is 6 orders of magnitude higher than the detectivity previously reported for hybrid perovskite-graphene photodetectors.[4]

*Estimation of photomultiplication.* For our device presented in figure 2d 3 pW 633 nm light illumination generates 6 µA photocurrent. A single photon energy at 633 nm is 3.138 144 689x10$^{-19}$ J thus 3 pW illumination 9559789 phonons/second. 6 µA current is a flow of 3.7446x10$^{13}$ electron/sec by definition. Accordingly 1 incoming phonon is transformed to ~4x10$^{6}$ electrons in the device. This value is equivalent to 0.6 pA current in 1 photon/sec illumination conditions.

*Comparative table of the performances of the best-in-class graphene and* $MAPbI_3$ *photodetectors*

| Active Material | Spectral Window [nm] | Incident Power | Responsivity [A/W] | $V_G$ [V] | $V_{SD}$ [V] | Reference |
|---|---|---|---|---|---|---|
| ME-SLG/ PbS QDs | 532 | 8fW | ~$5x10^7$ | -20 | 5 | G. Konstantatos, et al.[5] |
| ME-SLG/ ME-$MLMoS_2$ | 635 | 6.4fW$\mu m^{-2}$ ~320fW | ~$5x10^8$ | -50 | 0.1 | K. Roy, et al. [6] |
| CVD-SLG/ $MAPbI_3$ NPs | 520 | 1µW | 180 | 0 | 0.1 | Y. Lee, et al. [4] |
| $MAPbI_3$ NPs | 365 | 10 µW$cm^{-2}$ | 3.49 | 0 | 3 | X. Hu et al. [7] |
| $MAPbI_3$ NWs | 633 | 340nW | $5x10^{-3}$ | 0 | 1 | E. Horváth et al. [2] |
| ME-SLG | 532 | - | $8.6x10^{-3}$ | 0 | 0.1 | Y. Zhang et al.[8] |
| CVD-SLG/ $MAPbI_3$ NWs | 633 | ~3 pW | ~$2x10^6$ | 0 | 0.01 | This work |

# References

[1] X. Li, Y. Zhu, W. Cai, M. Borysiak, B. Han, D. Chen, R. D. Piner, L. Colombo, R. S. Ruoff, Nano Letters 2009, 9, 4359.
[2] E. Horváth, M. Spina, Z. Szekrényes, K. Kamarás, R. Gaal, D. Gachet, L. Forró, Nano Letters 2014, 14, 6761.
[3] L. Dou, Y. Yang, J. You, Z. Hong, W.-H. Chang, G. Li, Y. Yang, Nat Commun 2014, 5.
[4] Y. Lee, J. Kwon, E. Hwang, C.-H. Ra, W. J. Yoo, J.-H. Ahn, J. H. Park, J. H. Cho, Advanced Materials 2015, 27, 41.
[5] G. Konstantatos, M. Badioli, L. Gaudreau, J. Osmond, M. Bernechea, F. P. G. de Arquer, F. Gatti, F. H. L. Koppens, Nat Nano 2012, 7, 363.
[6] K. Roy, M. Padmanabhan, S. Goswami, T. P. Sai, G. Ramalingam, S. Raghavan, A. Ghosh, Nat Nano 2013, 8, 826.
[7] X. Hu, X. Zhang, L. Liang, J. Bao, S. Li, W. Yang, Y. Xie, Advanced Functional Materials 2014, 24, 7373.
[8] B. Y. Zhang, T. Liu, B. Meng, X. Li, G. Liang, X. Hu, Q. J. Wang, Nat Commun 2013, 4, 1811.